electronics

MDPI

Article

Phase Stabilization of a Terahertz Wave Using Mach–Zehnder Interference Detection

Amalina Athira Ibrahim *, Bo Li, Shenghong Ye, Takashi Shiramizu, Hanwei Chen, Yuya Mikami and Kazutoshi Kato *

Graduate School of Information Science and Electrical Engineering, Kyushu University, Fukoka 819-0395, Japan; li.bo.641@s.kyushu-u.ac.jp (B.L.); ye.shenghong.983@s.kyushu-u.ac.jp (S.Y.); shiramizu.takashi.050@s.kyushu-u.ac.jp (T.S.); chen.hanwei.816@s.kyushu-u.ac.jp (H.C.); mikami@ed.kyushu-u.ac.jp (Y.M.)

* Correspondence: ibrahim.amalinaathira.206@s.kyushu-u.ac.jp (A.A.I.); kato@ed.kyushu-u.ac.jp (K.K.)

Abstract: As a high-frequency carrier, the terahertz (THz) wave is essential for achieving high-data-rate wireless transmission due to its ultra-wide bandwidth. Phase stabilization becomes crucial to enable phase-shift-based multilevel modulation for high-speed data transmission. We developed a Mach–Zehnder interferometric phase stabilization technique for photomixing, which has proved a promising method for phase-stable continuous THz-wave generation. However, this method faced inefficiencies in generating phase-modulated THz waves due to the impact of the phase modulator on the phase stabilization system. By photomixing, which is one of the promising methods for generating THz waves, the phase of the generated THz waves can be controlled in the optical domain so that the stability of the generated THz wave can be controlled by photonics technologies. Thus, we devised a new phase stabilization approach using backward-directional lightwave, which is overlapped with the THz wave generation system. This study presented a conceptual and experimental framework for stabilizing the phase differences of optical carrier signals. We compared the optical domain and transmission performances between forward-directional and backward-directional phase stabilization methods. Remarkably, our results demonstrated error-free transmission at a modulation frequency of 3 Gbit/s and higher.

Keywords: terahertz wave; phase stabilization; photomixing; optical frequency comb; phase modulator; phase modulation

Citation: Ibrahim, A.A.; Li, B.; Ye, S.; Shiramizu, T.; Chen, H.; Mikami, Y.; Kato, K. Phase Stabilization of a Terahertz Wave Using Mach–Zehnder Interference Detection. *Electronics* **2023**, *12*, 3366. https://doi.org/10.3390/electronics12153366

Academic Editors: Chao-Yang Lee, Neng-Chung Wang and Tien-Wen Sung

Received: 7 July 2023
Revised: 29 July 2023
Accepted: 2 August 2023
Published: 7 August 2023

1. Introduction

In recent times, the exponential surge in mobile data traffic necessitated the need for communication systems capable of handling higher frequency signal carriers, such as terahertz (THz) waves [1–7]. Positioned between radio waves and infrared waves, THz waves occupy a frequency range spanning from 0.1 to 10 THz. This unique range falls within the spectrum of capabilities that lie between traditional radio frequency (RF) and optical systems. Significantly surpassing the frequencies of radio waves, THz waves empower the transmission of communication signals with ultra-wide bandwidth [8–11]. Consequently, there has been an increasing interest among researchers and industry experts to explore the potential of terahertz frequencies as a practical solution for meeting the bandwidth demands of high-speed wireless communications [9–14].

There has been a race to boost data rates in response to rising demands and the need to improve service capabilities. Increasing data rates is critical to meet the ever-increasing service demands. This behavior is consistent with Edholm's Law, according to which bandwidth and data rates double every 18 months. This equation has been shown to be astonishingly accurate in forecasting the continued improvement of data transmission speeds. Wireless transmission rates were roughly 5 to 10 kbit/s in 1995 but had greatly increased to 100 kbit/s by 2004 [15]. During the shift from 3G to 4G LTE technologies

between 2000 and 2010, data rates ranged from several Mbit/s, with 4G LTE enabling download speeds of up to 100 Mbit/s between 2010 and 2020. Today, the implementation of 5G networks is predicted to reach speeds of up to 10 Gbit/s, as shown in Figure 1, in accordance with Edholm's law. Furthermore, the industry hopes to reach a peak data throughput of 1000 Gbit/s (1 Tbit/s) in 6G by 2035.

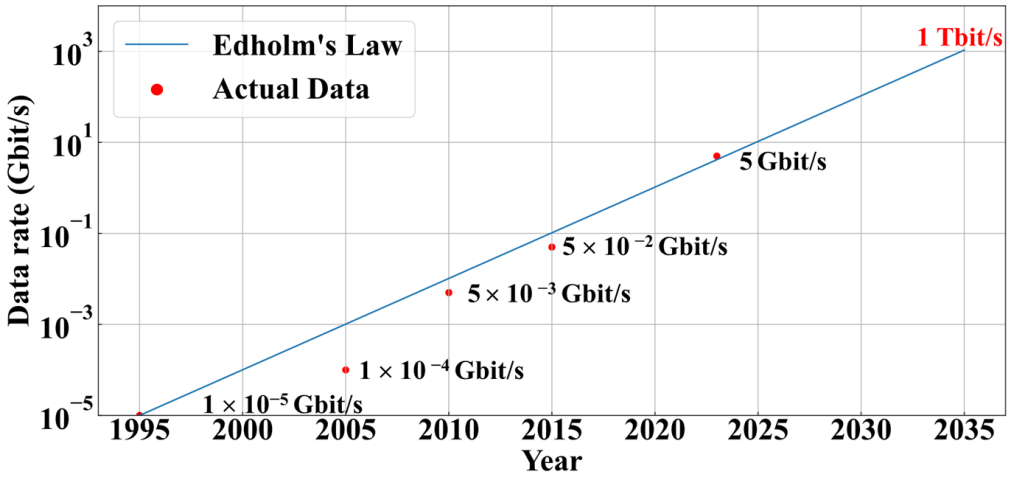

Figure 1. Wireless communication data rates from 1995 until 2035.

2. THz Waves: Meeting High-Speed Communication Needs

The introduction of terahertz frequencies into wireless communications opens up new possibilities for achieving high data rates and ultra-wide bandwidths. Regarding generating THz waves, two main approaches have been utilized: the all-electronics and optoelectronics approaches. The all-electronics approach involves employing electronic devices, such as high electron mobility transistors (HEMTs) and complementary metal-oxide-semiconductor (CMOS) technology, for both the THz emitter and receiver components [16,17]. This approach takes advantage of the capabilities of electronic devices to generate and detect THz waves. On the other hand, the opto-electronics approach which based on photonic generation on a high data rate THz signal. There are some approaches, such as Photonic Integrated Circuits (PICs) [18], Quantum Cascade Lasers (QCLs) [19], and photomixers or photodiodes [20].

We summarize up-to-date research efforts on the progress of high-speed THz wireless communication systems [21–34], as shown in Figure 2. The symbols used in the scatter plot correspond to various modulation schemes utilized in different research projects, while the colors distinguish the different approaches adopted by researchers. In the footprint map, carrier frequencies have been increased up to 500 GHz in order to explore more available bandwidth in higher frequency bands for carrying high-speed information. We can see that opto-electronic techniques have considerably contributed to higher data rates, particularly those over 80 Gbit/s. According to the graph, frequencies above 300 GHz are mostly handled utilizing opto-electronic techniques. The greatest transmission bit rate of 110 Gbit/s has been reached among all-electronics approaches at 240 GHz [35], while the opto-electronics approach has hit 140 Gbit/s at 500 GHz [36].

The all-electronics approach relies solely on electronic devices. This approach offers notable advantages, such as high resolution in accurately process and manipulate signals and high flexibility for THz applications. However, as electronic components operate at higher frequencies, they face challenges such as limited bandwidth, increased noise levels, and power consumption issues [37]. These limitations hinder their ability to keep pace with the exponentially growing demand for high-speed data transmission [38]. To overcome these challenges, photonics-based methods can provide a solution with wider bandwidths [39]. Unlike the all-electronics approach, the photonics approach utilizes a fiber optic configuration, enabling seamless connectivity between fiber optic and wireless

communication networks. By utilizing fiber optics, the photonics approach holds the potential for generating THz waves with wider bandwidths for higher-speed data transmission compared to purely electronic methods.

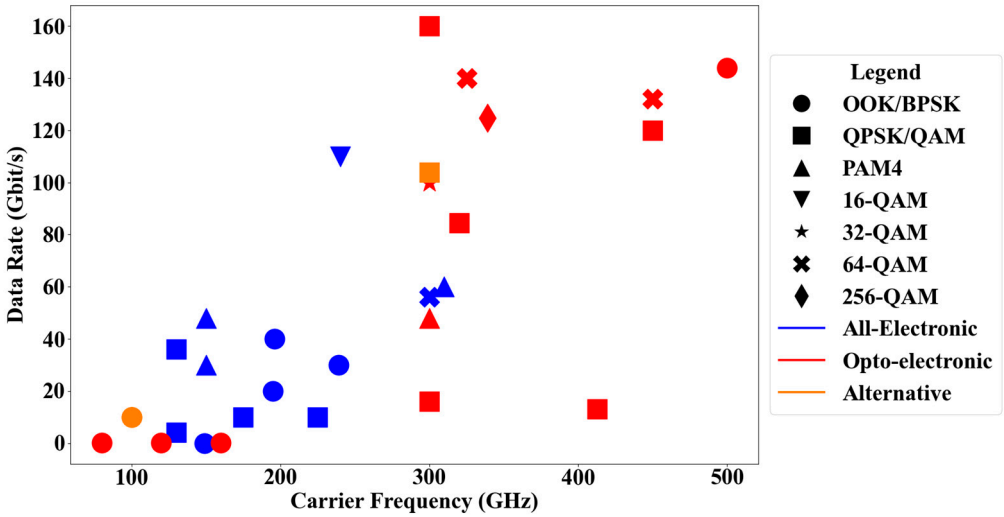

Figure 2. Data rate versus carrier frequency in the range of 100–500 GHz.

Among the various photonics approaches for generating THz waves, photomixing emerged as a promising technique [40–44]. Photomixing involves introducing two lightwaves with different frequencies onto a photoelectronic conversion device, such as a uni-traveling-carrier photodiode (UTC-PD) [45]. This technique exploits the square-law detection of the photoelectronic conversion device to generate high-frequency electrical signals in the THz range. The combination of the two input lightwaves generates a new signal in the THz frequency range.

3. Photomixing: A Photonic-Based Approach

Photomixing gained attention due to its ability to achieve high-frequency THz wave generation with excellent spectral purity and wide tunability. The UTC-PD, as a photomixer, is a key component in this technique, where it converts the optical power of the input lightwaves into a current. Introducing two continuous lightwaves with different frequencies of f_1 and f_2 into the photomixer resulted in the generation of THz waves. Let us say the initial lightwave is given below,

$$E_1 = A_1\, e^{i(2\pi f_1 t + \varphi_1)} \tag{1}$$

$$E_2 = A_2\, e^{i(2\pi f_2 t + \varphi_2)} \tag{2}$$

the frequency and phase of the generated THz wave depend on the frequency difference of $f_1 - f_2$ and the phase difference of $\varphi_1 - \varphi_2$ between the original two lightwaves, as shown in the equation below.

$$E_{THz} \propto |E_1 + E_2|^2 \propto {A_1}^2 + {A_2}^2 + 2A_1A_2\cos(2\pi(f_1 - f_2)t + (\varphi_1 - \varphi_2)) \tag{3}$$

One advantage of photomixing is offering a flexible and tunable approach to THz wave generation. By adjusting the frequencies of the input lightwaves, the generated THz frequency can be controlled, allowing for versatile applications in different communication scenarios. However, despite its promise, photomixing faces challenges that need to be addressed for practical implementation. One significant challenge is the phase stability of the lightwave, particularly for implementing multilevel phase modulation. Figure 3 shows an optical frequency comb (OFC)-based photomixing technique for THz wave generation [46,47]. In this technique, two lightwaves, whose optical frequencies are denoted

as f_1 and f_2, are extracted from the OFC using an optical filter. The extracted lightwaves are then combined using an optical coupler (OC). Although the initial phase locking of f_1 and f_2 is achieved, the generated THz wave may experience phase fluctuations, φ_{noise}, due to path length variations in the optical fibers between the optical filter and the OC. This situation is due to the total phase difference of the generated THz wave will always change based on the φ_{noise}, as shown in the equation below.

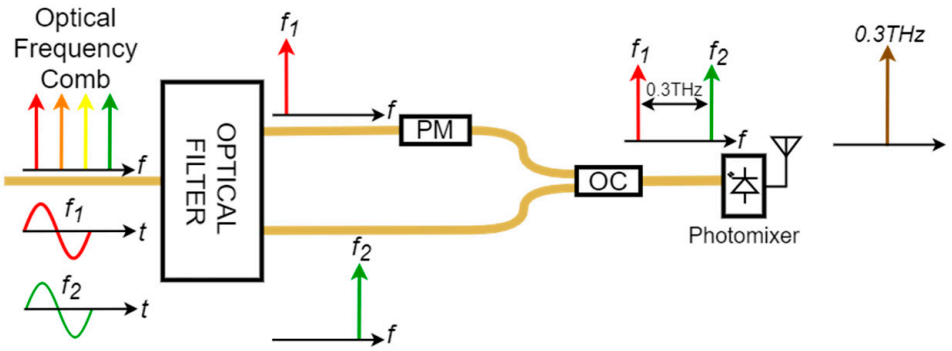

Figure 3. OFC-based technique of photomixing.

$$E_{THz} \propto A_1{}^2 + A_2{}^2 + 2A_1A_2\cos(2\pi(f_1 - f_1)t + (\varphi_1 - \varphi_2 + \varphi_{noise})). \quad (4)$$

Therefore, phase stabilization techniques for the lightwaves are necessary to ensure the stability and reliability of the THz wave generated through photomixing.

4. Phase Stabilization Method

In previous research, we developed a phase stabilization system using the Mach–Zehnder Interferometric (MZI) phase stabilization method [48–50]. This method involved introducing a pilot lightwave, f_0, into the THz-wave intensity-modulation (IM)/coherent detection (CD) system, which can be considered an MZI, as shown in Figure 4. As the pilot lightwaves from the upper and lower path interfere after OC, the interference signal is detected. This interference signal that represented the φ_{noise} is then converted into an electrical signal and introduced into the feedback controller. By controlling the intensity of the interfered pilot lightwave at a constant, the stabilization of the THz-wave IM system was achieved.

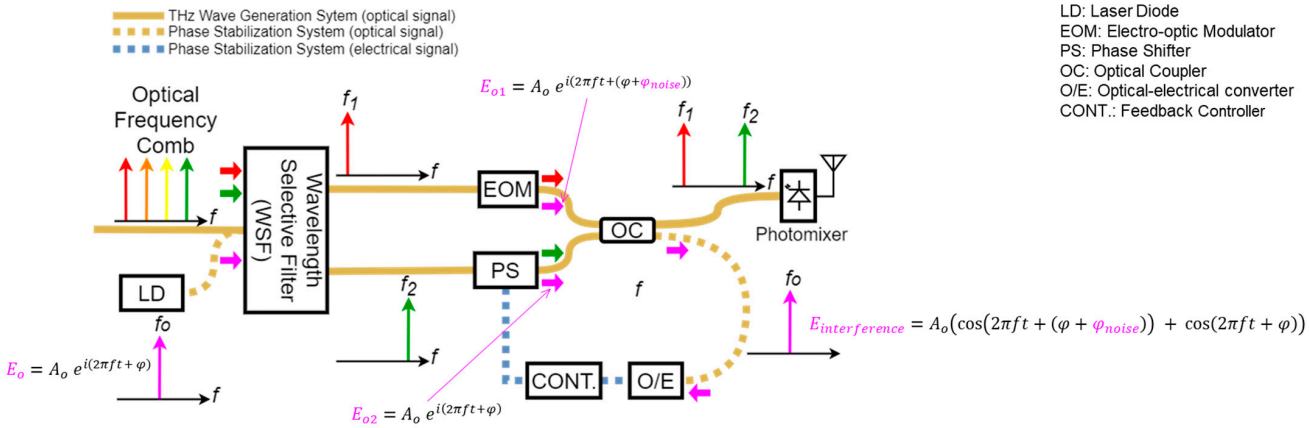

Figure 4. MZI phase stabilization method.

This approach successfully demonstrated the transmission of THz-wave data using IM/CD. However, it is important to note that this method is not suitable for THz-wave phase modulation (PM), which is necessary for implementing multilevel PM schemes such as quadrature phase shift keying (QPSK) or 16-state quadrature amplitude modulation

(16QAM) for higher data rates. The pilot lightwave used in the MZI-based stabilization system would also undergo phase modulation, making it unable to accurately detect and compensate for phase fluctuations.

To address this limitation, the pilot lightwave was introduced along a backward direction. Figure 5 illustrates the use of a 100 mm-long lithium niobate (LN) phase modulator to modulate the phase of lightwaves [51]. The modulation is achieved by applying an electrical signal to the traveling-wave electrode of the LN modulator, causing a shift in the phase of the lightwave passing through it. Here, if the bit length is shorter than the length of the phase modulator, the optical lightwave traveling in the backward direction will not undergo modulation. This situation occurs because the lightwave encounters a constantly switching electrical signal voltage, resulting in the phase shift being effectively averaged out and remaining unaffected. However, it should be noted that the longer electrical bit would modulate the pilot lightwave.

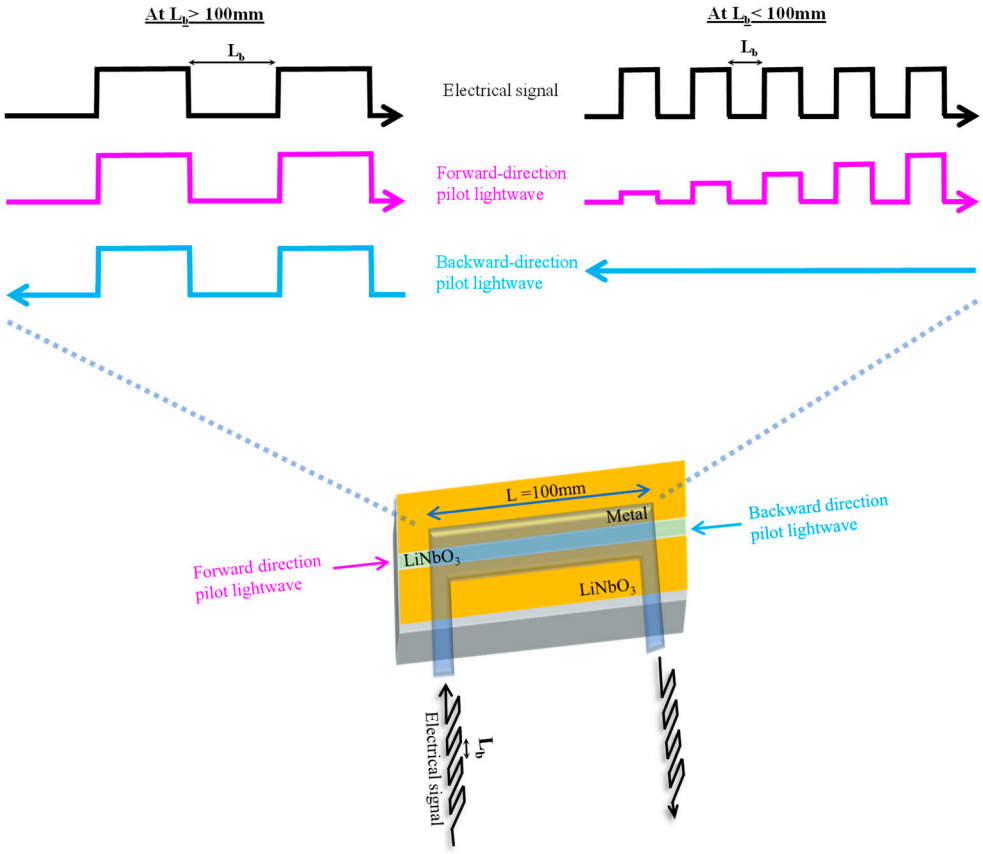

Figure 5. Illustration of LN phase modulator and the phase modulation of the pilot lightwave.

Consequently, no significant modulation is observed on the backward pilot lightwave. In the case where the bit length (L_b) of the electrical signal is shorter than the length of the phase modulator (L), denoted as $L_b < L$, the backward pilot lightwave encounters a constantly fluctuating electrical signal voltage. This fluctuation can be represented by a time-varying function $V(t)$, which represents the voltage applied to the phase modulator at time t with constant k. Considering the phase modulation equation $\Delta\varphi \propto kVL$, we can express the phase shift experienced by the backward pilot lightwave as:

$$\Delta\varphi_{\text{backward}}(t) \propto kV(t)L_b. \quad (5)$$

Since $V(t)$ constantly switches within the short bit length, the integral of $V(t)$ over that duration is expected to be averaged. Therefore, the phase shift $\Delta\varphi_{\text{backward}}$, which the

backward lightwave experienced, can be effectively averaged out as well, resulting in no significant phase modulation:

$$\Delta\varphi_{\text{backward}} \propto \int \{kV(t)L\}dt \approx 0. \quad (6)$$

In the following two sections, phase detection and stabilization in the optical domain using forward-direction and backward-direction pilot lightwaves are presented and the stability of phase-modulated THz-wave data transmission is discussed.

5. Phase Detection and Stabilization System of the Optical Domain

We constructed an experimental setup to further explore the phase detection and stabilization techniques in a THz-wave phase PM system. Building upon the earlier discussed issues, our current focus is to compare the phase stabilization system based on the MZI technique by using the performance of forward and backward-direction pilot lightwaves. By introducing a pilot lightwave into two optical paths, the combined lightwaves at the output coupler will experience interference. By carefully controlling the intensity of the interfered lightwave, we can maintain a constant phase difference between the lightwaves of the two optical paths. This comparative study aims to evaluate the stability and reliability of phase stabilization system methods in stabilizing the THz wave generation system, which depends on the direction of the pilot lightwave being introduced into the system. In the forward-direction phase stabilization system, the pilot lightwave passes from the input of the THz wave generation system. In contrast, in the backward-direction phase stabilization system, the pilot lightwave travels from the output of the THz wave generation system. This setup allows us to study the impact of the pilot lightwave direction on the stability of the system.

5.1. Experimental Setup

5.1.1. Forward-Direction Pilot Lightwave System

Figure 6 illustrates the block diagram of a reference experiment conducted to generate phase-modulated THz waves using a forward pilot lightwave in the phase stabilization system. In this THz-wave PM generation system (solid line), a single lightwave with a frequency f_{gen} of 193.4125 THz (orange arrow) was introduced from the left side instead of utilizing two lightwaves with different optical frequencies. The introduced lightwave underwent amplification by an Erbium-Doped Fiber Amplifier (EDFA). After the EDFA, the lightwave passed through an isolator to ensure unidirectional transmission and suppress any unwanted reflections or backscattering effects. The lightwave was split into two optical paths at the optical splitter (OS). This point was marked as the input of the MZI. The upper path involved the lightwave traveling through a traveling-wave optical phase modulator (OPM) and being phase-modulated by the pulse pattern generator (PPG) at rates of 1, 3, and 10 Gbit/s using a constant pseudorandom binary sequence (PRBS) of length 2^7-1. The lower path comprised the lightwave passing through the phase shifter (PS). The lightwaves from these two paths were combined at the OC, and were marked here as the output of the MZI. Figure 6 also shows the optical spectra of the input and output lightwaves into the MZI. The input power of the f_{gen} into the MZI was -12 dBm and the output was -2.42 dBm. The observed loss may result from various factors in our complex experimental setup, including fiber-to-waveguide connections, as well as certain devices that introduce considerable inefficiencies. The coupled signal was introduced to an optical-electrical (O/E) converter, resulting in the modulated signal. The phase stability of modulated signal in the THz-wave generation system was observed by comparing it with the initial signal injected into the OPM using an OSC and a bit error rate tester (BERT) simultaneously.

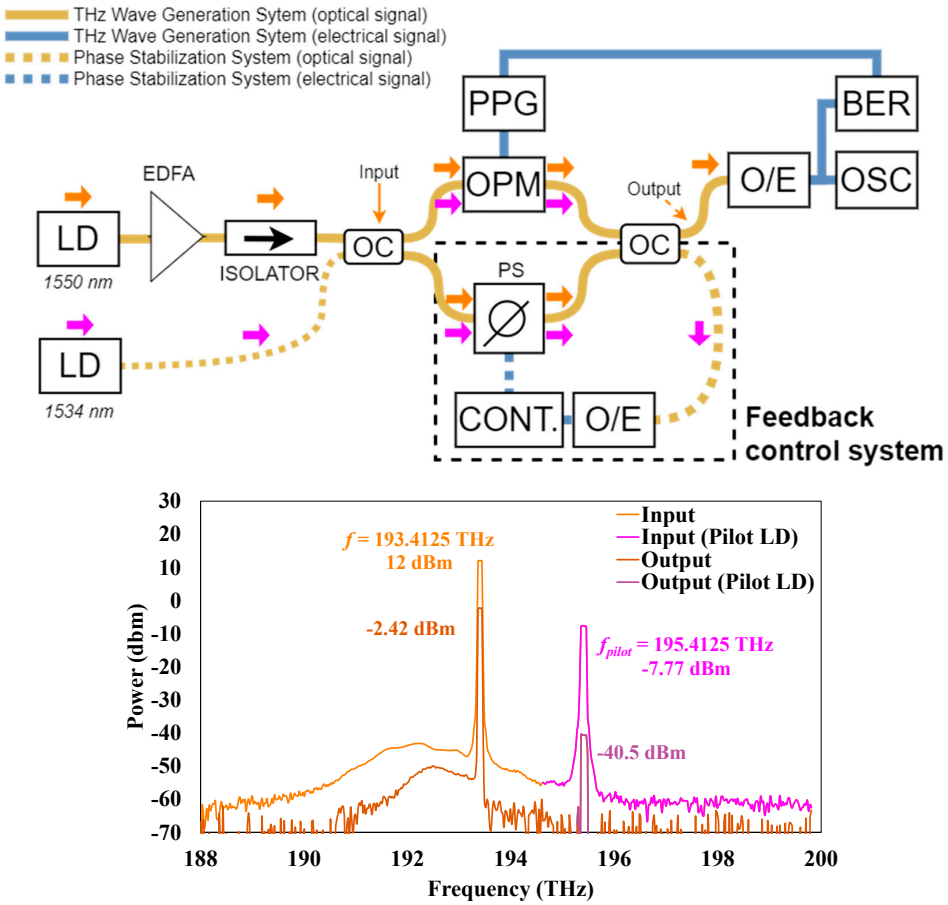

Figure 6. Experimental setup of phase stabilization systems with forward-direction pilot lightwave and the optical spectra at the input and the output of the system.

In contrast, the phase stabilization system (dotted line) operated as follows: the pilot lightwave (pink arrow) originated from a laser with an optical frequency of 195.4125 THz. The frequency of the pilot lightwave was purposely chosen to be different from the frequency used in the THz wave generation system to avoid interference between the two signals. The pilot lightwave was then input into the MZI configuration at the OC. The lightwave was split and directed through the upper path involving the OPM and the lower path involving the PS. As shown in Figure 6's optical spectra graph, the input pilot lightwave into the THz wave generation had a power of −7.77 dBm while the output was −40.5 dBm. The pilot lightwave at the output of the THz wave generation system was of negligible magnitude, and its influence on the generation process was inconsequential, rendering it a non-issue. Instead, after coupling at the OC, the pilot lightwaves interfered and passed through the other arm of the coupler to the O/E converter. The interference of the pilot lightwave enabled the detection of phase fluctuations occurring by phase changes in the optical paths, particularly the optical fiber. The intensity of the interference was then measured using the O/E converter. The converted voltage was subsequently read by a feedback controller, which adjusted the PS to maintain a constant voltage detected at the O/E converter. By precisely controlling and maintaining the intensity of the interfered pilot lightwave, the phase fluctuations in the THz wave generation system can be effectively eliminated, enabling the application of a high-sensitivity coherent detection at the output of the THz wave generation system.

5.1.2. Backward-Direction Pilot Lightwave System

Figure 7 shows the experimental setup featuring a phase stabilization system utilizing a backward-direction pilot lightwave. Similar to the forward-direction pilot lightwave

system, a single lightwave was employed in the THz-wave PM generation system (solid line). The input power of a lightwave with a frequency f_{gen} of 193.4125 THz into the THz wave generation system was 14.5 dBm, and the output was −3.28 dBm, as shown in Figure 7 optical spectral graph. The configuration of the phase stabilization system (dotted line) was positioned on the right side. In this setup, the pilot lightwave (light blue arrow) was introduced to the THz wave generation system from the output of the setup. It was observed that the power of the pilot lightwave at the output of the THz wave generation system was −41.9 dBm, which was primarily due to the effects of total internal reflection at the OC (output). However, this power value was negligible and can be disregarded as it did not significantly impact the THz wave generation system. The pilot lightwave traveled through the lower arm of the OC and split into two paths. In the upper path, it passed through the OPM along the opposite direction, while in the lower path, it passed through the PS. Then, the pilot lightwave was recoupled after the OC (input). The coupled pilot lightwave was detected by the O/E converter. As the OPM modulated the phase of the lightwave only when the lightwave and the electrical data signal traveled in the same direction, the phase of the backward-direction pilot lightwave remained unmodulated. Hence, efficient interference was expected in this configuration.

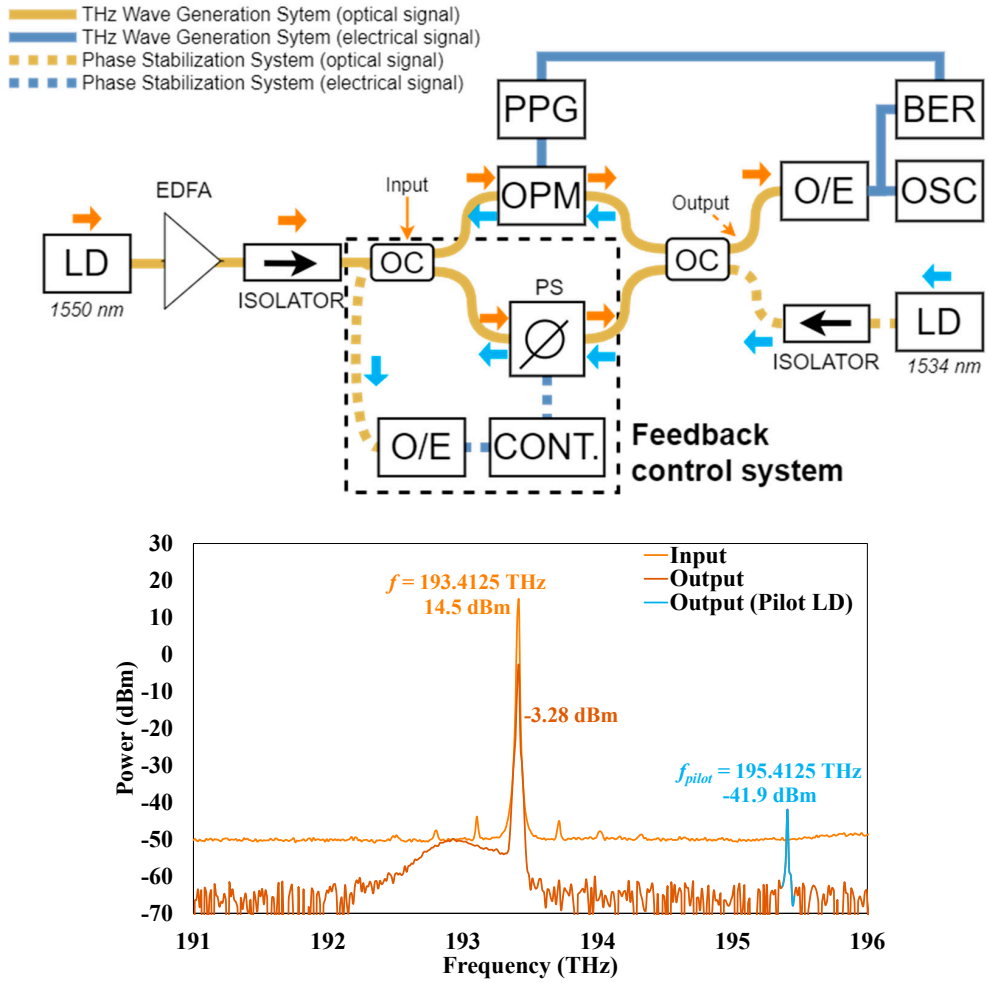

Figure 7. Experimental setup of phase stabilization systems with backward-direction pilot lightwave and the optical spectra at the input and the output of the system.

5.2. Detected Interference Intensity

Next, we observed the stabilization of the interfered intensity of the pilot lightwave, as depicted in Figure 8a,b. These figures present the voltage readings obtained from the O/E converter of the phase stabilization system, which indicate the interfered intensity of both

the forward-direction and backward-direction pilot lightwaves in the presence and absence of the phase stabilization system. The measurements were performed at various bit rates applied to the OPM; 1, 3, and 10 Gbit/s. Figure 8a shows the interference voltage value over time for the forward-direction pilot lightwave in the case of the system OFF and ON. The interference voltage displayed instability and fluctuations without the activation of the phase stabilization system. And, even with the activation of the phase stabilization system, the interfered intensity failed to maintain a constant voltage across all modulation bit rates. The condition happened in all modulation rates, 1, 3, and 10 Gbit/s. This behavior can be attributed to the blurring effect induced by the modulation of the pilot lightwave within the phase modulation system itself.

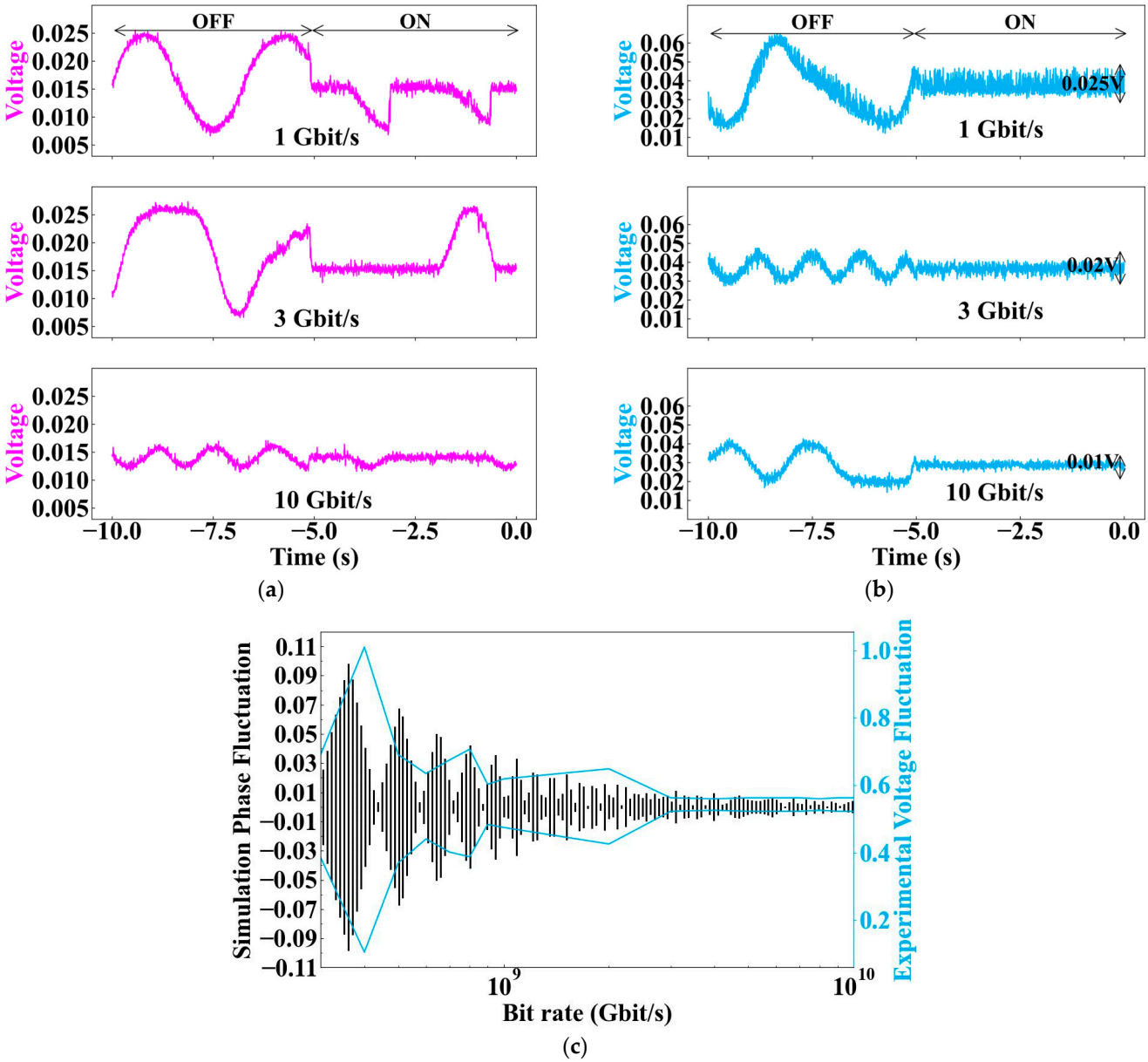

Figure 8. The detected interference intensity for (**a**) forward-direction pilot lightwave and (**b**) backward-direction pilot lightwave. (**c**) Simulation result of phase fluctuation of the backward-direction pilot lightwave.

In contrast, when employing the phase stabilization system with a backward-direction pilot lightwave, the interfered intensity achieved stability when the phase stabilization

was ON, as shown in Figure 8b. Furthermore, the vertical width of the interfered intensity, denoted as V_T, varied depending on the bit rate of the phase modulation. V_T decreased as the bit rate increased, indicating a reduced impact of phase modulation on the pilot lightwave at higher bit rates. At modulation bit rates of 3 Gbit/s and higher, the voltage fluctuation achieved a stable state with minimal fluctuations, measuring less than 0.02 V. In comparison, at 1 Gbit/s, the voltage fluctuation was 0.025 V. These results suggest that the phase modulation had minimal impact on the pilot lightwave at bit rates exceeding 3 Gbit/s. These experimental findings aligned with our simulation results displayed in Figure 8c and validated the effectiveness of the backward-direction phase stabilization system. The simulation result did show the probability of the phase fluctuation of the pilot lightwave that passed through the phase modulator in the backward direction. It shows that the phase fluctuation became smaller as the modulation bit rate increased. Notably, at 3 Gbit/s, the phase fluctuation was significantly small. The behavior was also the same as the experimental voltage fluctuation.

These results are significant as they demonstrated the effectiveness of the phase stabilization system using a backward-direction pilot lightwave in maintaining stable interfered intensity. By toning down the fluctuations and achieving stability, this approach enables improved performance in generating phase-modulated THz waves. Furthermore, the observed variations in V_T provide insights into the influence of bit rates on the impact of phase modulation on the pilot lightwave. This analysis can guide the optimization of generation system configurations for enhanced THz-wave communication systems.

5.3. Stability of the Optical Domain

Then, the phase stability of the optical domain was assessed by observing the eye pattern at different bit rates of 1, 3, and 10 Gbit/s. A comparison of the performance between the forward-direction and backward-direction phase stabilization systems is presented in Figure 9a,b, respectively. In both figures, the blue dots represent the original modulation data from the PPG as a reference, while the orange dots represent the detected signal. It is clear that the forward-direction phase stabilization system failed to achieve a stable eye-opening at each bit rate. In the case of the backward-direction phase stabilization system, at lower bit rates, the pilot lightwave still underwent modulation and could not be interfered with, thus preventing feedback control for phase stabilization.

Consequently, the resulting eye pattern exhibited an unclear eye-opening. On the other hand, a clear eye-opening was achieved at bit rates exceeding 3 Gbit/s. These findings provide experimental evidence supporting the effectiveness of phase stabilization using a backward-direction pilot lightwave, particularly at higher bit rates, thereby agreeing with our earlier theoretical predictions.

Afterward, the bit-error-rate (BER) characteristics during data transmission were investigated by varying the bit rates of the modulation in the THz wave generation system. Figure 9c displays the BER as a function of THz wave generation. With the forward-direction phase stabilization system, the BER remained largely unchanged and consistently stayed close to 10^0. In contrast, the BER showed a significant decrease with the backward-direction phase stabilization system. These experimental results clearly demonstrate the adaptability and efficacy of the phase stabilization system employing the backward-direction pilot lightwave for the THz-wave generation system.

The observed improvements in eye pattern stability and reduced bit-error rates underscore the importance of employing the appropriate pilot lightwave direction in achieving robust and reliable phase stabilization, especially at higher bit rates. Such improvements are crucial for realizing multilevel phase modulation for a higher data-rate transmission in THz-wave applications.

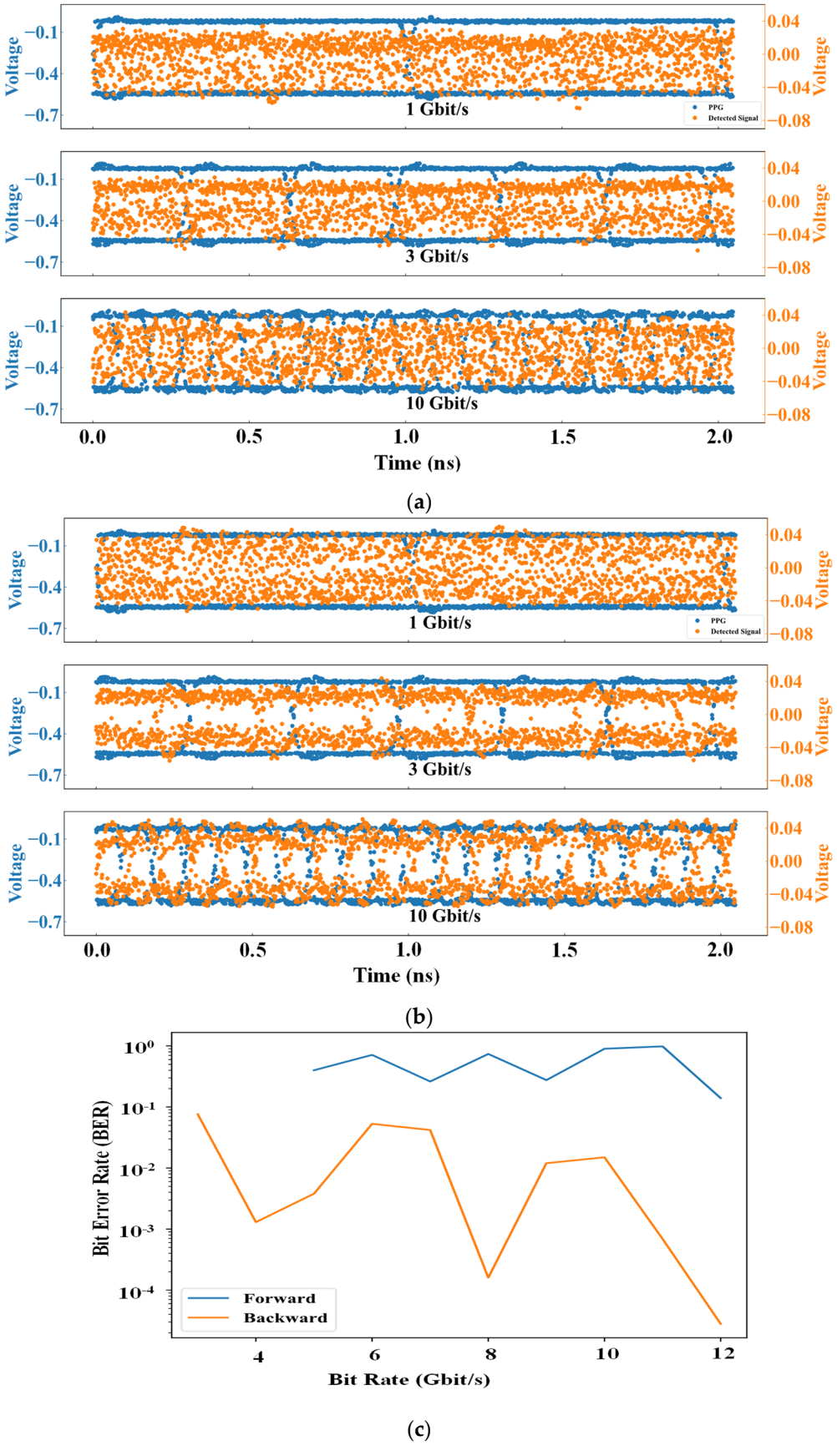

Figure 9. The eye pattern of the optical domain experimental setup with (**a**) forward-direction pilot lightwave and (**b**) backward-direction pilot lightwave at 1, 3 and 10 Gbit/s and (**c**) BER versus bit rate of optical domain THz wave generation system.

6. THz-Wave Generation System

In this section, we explore the implementation of phase stabilization techniques in a phase-modulated THz-wave generation and transmission setup. Our experiment involved comparing both a forward-direction phase stabilization system and a backward-direction phase stabilization system. The configuration was divided into two parts: the transmitter part, $T_{X,}$ where we generated the THz wave through photomixing using two different lightwaves, and the receiver part, $R_{X,}$ where the detected THz wave was down-converted and observed.

The purpose of this setup was to demonstrate the practical application of the phase stabilization system in an actual THz generation system. We began by presenting the configuration of the experimental THz generation setup and applying a phase stabilization system. Then, we investigated the detected signal of the phase-modulated THz wave. Here, we present the experimental details that validated the effectiveness of the phase stabilization technique in the context of phase-modulated THz-wave generation. Through this analysis, we aim to contribute to the understanding and optimization of phase stabilization methods for THz wave PM applications.

6.1. Experimental Setup

6.1.1. THz-Wave Generation System with Forward-Direction Phase Stabilization System

Figure 10 illustrates the THz wave PM system equipped with a forward-direction phase stabilization system. The T_X initiated the process by introducing a single lightwave at a frequency of 193.4 THz from a laser diode (LD) on the left side of the configuration. An optical frequency comb generator (OFCG) generated a frequency comb with equally spaced spectral lines of 25-GHz spacing, allowing us to output specific optical frequencies with a 300 GHz difference at the wavelength selective filter (WSF). In the upper path, the lightwave (red arrow) underwent phase modulation using the OPM, employing a return-to-zero (RZ) continuous signal from the PPG. In the lower path (green arrow), the lightwave passed through the PS. The lightwaves from these two paths were combined at the OC, amplified, and directed to the UTC-PD, acting as a photomixer. The input and output power of the THz wave generation system can be observed in Figure 10's optical spectra graph. It shows that the output power of f_1 was -9.2 dBm, while the f_2 was -10.2 dBm. Achieving power balance is crucial to ensure that both signals contribute equally to the mixing process. Despite the power differences between these two frequencies, as depicted in the optical spectra, it is important to note that both frequencies had almost the same output power. This is because f_1 had undergone modulation, resulting in the total output power being equivalent to that of f_2. Consequently, the UTC-PD generated the phase-modulated THz wave, which was transmitted through the WR3.4 waveguide. As the carrier frequency of the THz signal is determined by the frequency difference between the lightwave, the output of the UTC-PD radiated a 300 GHz wave with 1, 5, and 10 Gbit/s Binary Phase-Shift Keying (BPSK) modulation.

At the R_X, a sub-harmonic mixer (SHM) was utilized to downconvert the received THz wave by a local oscillator (LO). The LO, with a frequency of 12.5 GHz from the signal generator (SG), was first multiplied by 12 using an electrical multiplier and then further multiplied by 2 inside the SHM, resulting in a total LO frequency of 300 GHz. This LO signal was also synchronized with the signal generator of the OFCG at the transmitter, enabling the implementation of homodyne detection. The resulting waveform was observed on an OSC.

In the phase stabilization system (dotted line), a pilot lightwave from a laser (pink arrow) with an optical frequency of 195.4125 THz was introduced to the THz-wave generation system. The pilot lightwave power at the input of the THz wave generation system was -8.44 dB and at the output was -43.4 dBm, which can be negligible to influence THz generation system, as shown in Figure 10's optical spectra graph. This pilot lightwave was then split and directed through the upper path involving the OPM and the lower path involving a PS. These lightwaves interfered after coupling at the OC, and the interference

intensity was detected by an O/E converter. The resulting converted voltage was then read by a feedback controller, which maintained a constant interference intensity by controlling the PS.

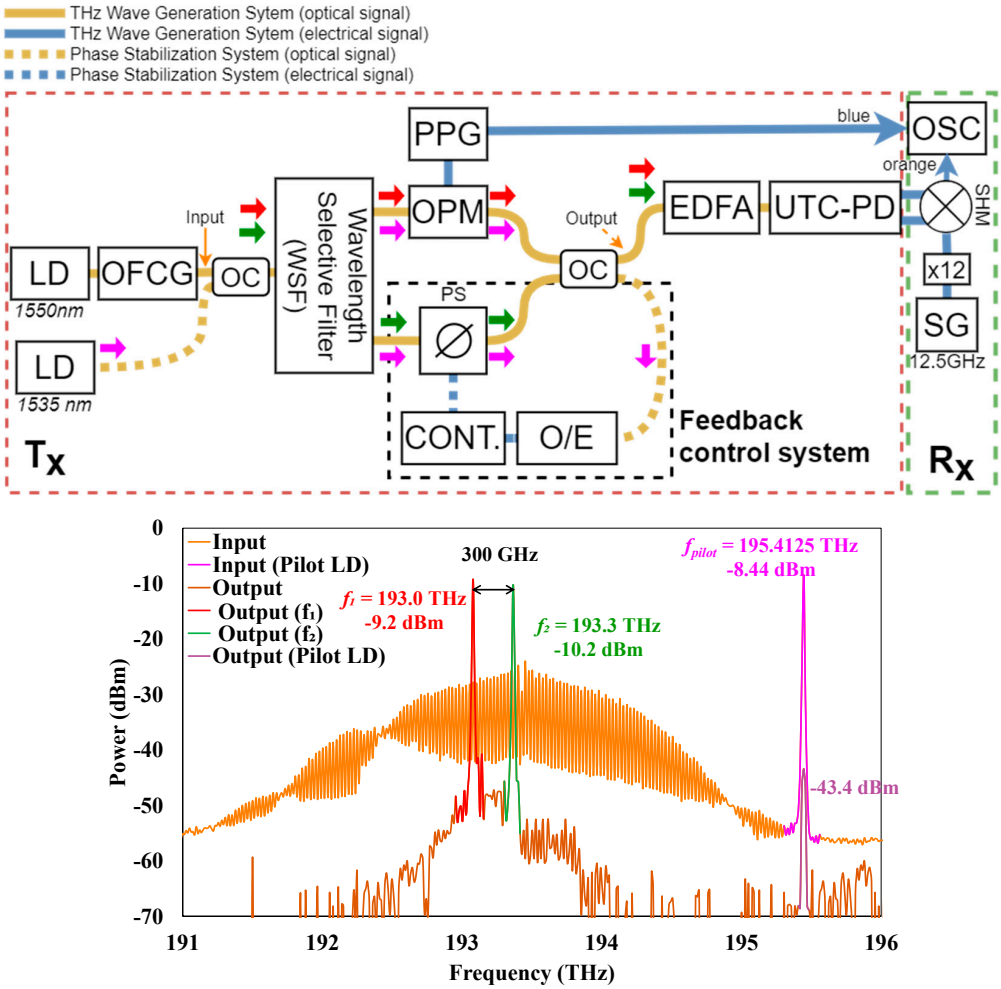

Figure 10. Experimental setup of THz wave generation system with forward-direction pilot lightwave and the optical spectra of input and output lightwaves of THz wave generation system.

6.1.2. THz-Wave Generation System with Backward-Direction Phase Stabilization System

Figure 11 depicts the THz wave PM system with the backward-direction phase stabilization system. This configuration utilized the lightwave in a manner similar to the forward-direction pilot lightwave system. This time, the output power of f_1 was −9.24 dBm, while the f_2 was −10.24 dBm, as shown in Figure 11's optical spectra graph. Moving on to the phase stabilization system, a pilot lightwave that originated from an LD was introduced from the right side of the THz wave PM system. The internal reflection at the OC caused the detection of the pilot lightwave at the output of the THz generation setup, but the power level was significantly low, measuring at −45.83 dBm. The pilot lightwave (light blue arrow) was split and then directed through the upper path involving the OPM and the lower path involving the PS in a backward direction. These lightwaves interfered after passing through the WSF in reverse. Due to the absence of phase modulation in the backward-direction pilot lightwave at bit rates of 3 Gbit/s and higher, efficient interference was anticipated. The interference intensity was detected using an O/E converter, and the resulting voltage was read by a feedback controller responsible for maintaining a constant interference intensity by controlling the PS.

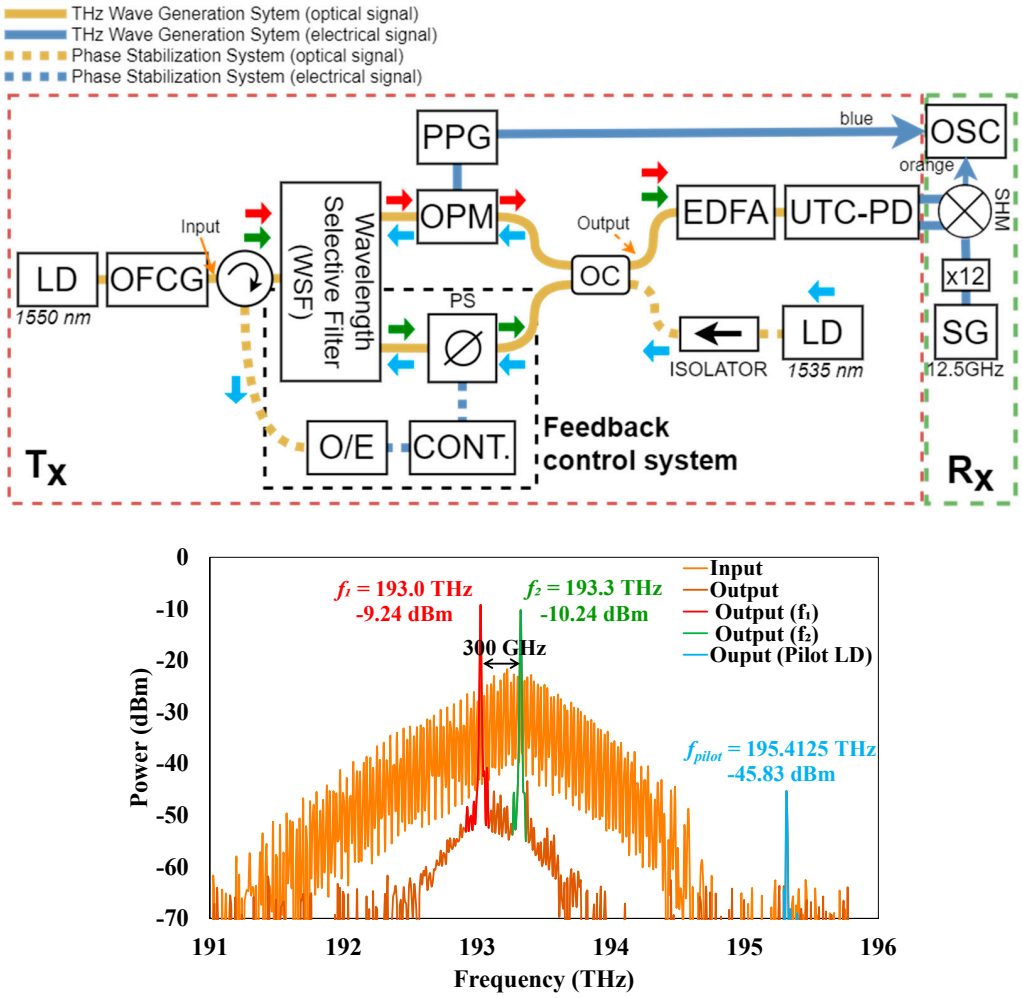

Figure 11. Experimental setup of THz wave generation system with backward-direction pilot lightwave and the optical spectra of input and output lightwaves of THz wave generation system.

6.2. Observation of Phase-Modulated THz Wave

We proceeded with the transmission of the phase-modulated 300-GHz wave and detected it using a sub-harmonic mixer equipped with a 300-GHz LO signal, employing coherent detection. Figure 12a,b present the detected waveforms (orange) alongside the initial modulation patterns generated by the PPG (blue) for forward-direction and backward-direction phase stabilization systems, respectively. The results demonstrate that the forward-direction phase stabilization system did not yield a distinct and continuous data pattern. In contrast, the backward-direction phase stabilization system exhibited a noticeable and continuous data pattern at bit rates of 5 and 10 Gbit/s and did not exhibit the same level of continuity at a lower bit rate of 1 Gbit/s. These experimental findings corroborate our previously established theoretical results. These observations provide valuable insights into the performance and limitations of the forward-direction and backward-direction phase stabilization systems in the context of phase-modulated THz wave transmission. The promising results obtained with the backward-direction system indicate its potential for supporting high-speed data transmission. These findings contribute to the efforts in optimizing and enhancing the stability and reliability of phase-modulated THz wave communication systems.

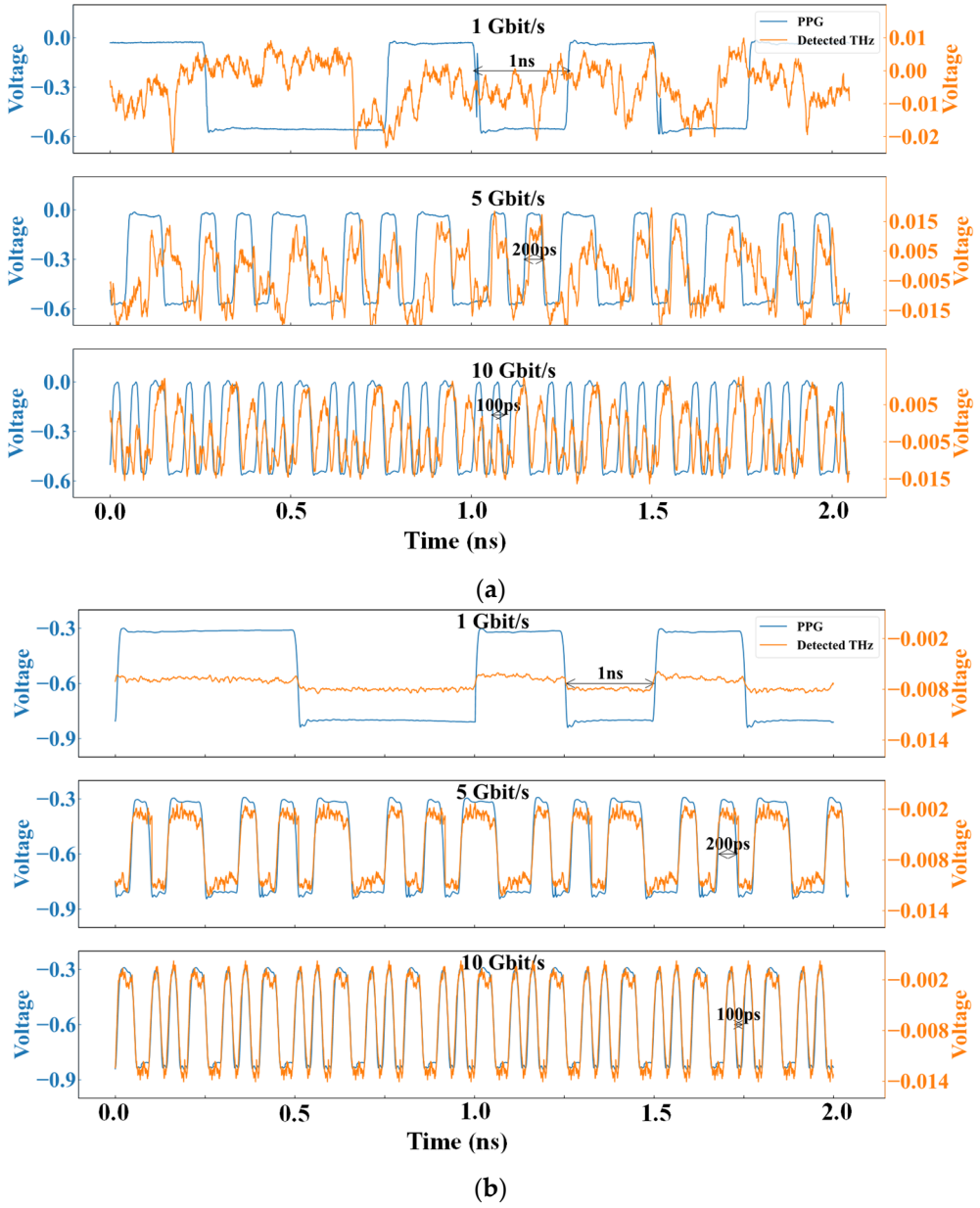

Figure 12. Detected phase-modulated THz signal with (**a**) forward-direction pilot lightwave and (**b**) forward-direction pilot lightwave at 1, 5 and 10 Gbit/s.

7. Conclusions

Our research successfully developed and compared a phase stabilization system for THz wave phase modulation using photomixing, employing both forward-direction and backward-direction approaches. The findings of our study highlighted the effectiveness of the backward-direction phase stabilization method in achieving stable phase fluctuations between the two lightwaves while eliminating the impact of environmental disturbances. As a result, we generated and transmitted a stable phase-modulated 300-GHz wave at a bit rate of 3 Gbit/s and beyond using the constructed system. This significant outcome provides evidence supporting the effectiveness of the backward-direction phase stabilization system. In addition to the significant outcomes of our study, there is room for further in the proposed phase stabilization method. Future investigations should focus on optimizing the system's performance to attain even higher bit rates and explore its robustness under various operating conditions.

Author Contributions: Data curation, A.A.I., B.L., S.Y., T.S., H.C., Y.M. and K.K.; methodology, A.A.I. and K.K.; writing—original draft preparation, A.A.I.; writing—review and editing, A.A.I., Y.M. and K.K. All authors have read and agreed to the published version of the manuscript.

Funding: This research was funded by the commissioned research by the National Institute of Information and Communications Technology (NICT) #02801, #00901 and the MIC/SCOPE #195010002, JSPS KAKENHI Grant Numbers: JP21K18730, JP20H00253.

Data Availability Statement: The datasets generated during and/or analyzed during the current study are available from the corresponding author on reasonable request.

Acknowledgments: The first author expresses sincere gratitude and appreciation to the Japan International Cooperation Agency (JICA) for providing a scholarship that enabled this research.

Conflicts of Interest: The authors declare no conflict of interest.

References

1. Cisco Systems, Inc. Cisco Visual Networking Index: Forecast and Trends, 2017–2022 White Paper. *Cisco Forecast Methodol.* **2019**, *17*, 13.
2. Akyildiz, I.F.; Kak, A.; Nie, S. 6G and Beyond: The Future of Wireless Communications Systems. *IEEE Access* **2020**, *8*, 133995–134030. [CrossRef]
3. Jia, W.; Liu, M.; Lu, Y.; Feng, X.; Wang, Q.; Zhang, X.; Ni, Y.; Hu, F.; Gong, M.; Xu, X.; et al. Broadband terahertz wave generation from an epsilon-near-zero material. *Light Sci. Appl.* **2021**, *10*, 11. [CrossRef]
4. Mashino, J.; Fujino, Y.; Kudo, R. R&D Activities of Core Wireless Technologies toward 6G Radio Access. *NTT Tech. Rev.* **2022**, *20*, 30–36.
5. Rappaport, T.S.; Xing, Y.; Kanhere, O.; Ju, S.; Madanayake, A.; Mandal, S.; Alkhateeb, A.; Trichopoulos, G.C. Wireless communications and applications above 100 GHz: Opportunities and challenges for 6g and beyond. *IEEE Access* **2019**, *7*, 78729–78757. [CrossRef]
6. Li, R. Huawei Towards a new internet for the year 2030 and beyond. In Proceedings of the 3rd Annual ITU IMT-2020/5G Workshop Demo Day, Geneva, Switzerland, 18 July 2018.
7. Akyildiz, I.F.; Han, C.; Hu, Z.; Nie, S.; Jornet, J.M. Terahertz Band Communication: An Old Problem Revisited and Research Directions for the Next Decade. *IEEE Trans. Commun.* **2022**, *70*, 4250–4285. [CrossRef]
8. Nikbakht, H.; Latifi, H.; Oraie, M.; Amini, T. Fabrication of Tapered Tip Fibers With a Controllable Cone Angle Using Dynamical Etching. *J. Light. Technol.* **2015**, *33*, 4707–4711. [CrossRef]
9. Boulogeorgos, A.A.A.; Alexiou, A.; Merkle, T.; Schubert, C.; Elschner, R.; Katsiotis, A.; Stavrianos, P.; Kritharidis, D.; Chartsias, P.K.; Kokkoniemi, J.; et al. Terahertz Technologies to Deliver Optical Network Quality of Experience in Wireless Systems beyond 5G. *IEEE Commun. Mag.* **2018**, *56*, 144–151. [CrossRef]
10. Song, H.J.; Lee, N. Terahertz Communications: Challenges in the Next Decade. *IEEE Trans. Terahertz Sci. Technol.* **2022**, *12*, 105–117. [CrossRef]
11. Huq, K.M.S.; Busari, S.A.; Rodriguez, J.; Frascolla, V.; Bazzi, W.; Sicker, D.C. Terahertz-Enabled Wireless System for Beyond-5G Ultra-Fast Networks: A Brief Survey. *IEEE Netw.* **2019**, *33*, 89–95. [CrossRef]
12. Elayan, H.; Amin, O.; Shihada, B.; Shubair, R.M.; Alouini, M.-S. Terahertz Band: The Last Piece of RF Spectrum Puzzle for Communication Systems. *IEEE Open J. Commun. Soc.* **2020**, *1*, 1–32. [CrossRef]
13. Han, C.; Yan, L.; Yuan, J. Hybrid Beamforming for Terahertz Wireless Communications: Challenges, Architectures, and Open Problems. *IEEE Wirel. Commun.* **2021**, *28*, 198–204. [CrossRef]
14. Singh, A.; Petrov, V.; Guerboukha, H.; Reddy, I.V.A.K.; Knightly, E.W.; Mittleman, D.M.; Jornet, J.M. Wavefront Engineering: Realizing Efficient Terahertz Band Communications in 6G and Beyond. *arXiv* **2023**, arXiv:2305.12636.
15. Cherry, S. Edholm's law of bandwidth. *IEEE Spectr.* **2004**, *41*, 58–60. [CrossRef]
16. Houston, P.A. High-frequency heterojunction bipolar transistor device design and technology. *Electron. Commun. Eng. J.* **2000**, *12*, 220–228. [CrossRef]
17. Jameson, S.; Socher, E. A 0.3 THz Radiating Active × 27 Frequency multiplier Chain with 1 mW Radiated Power in CMOS 65-nm. *IEEE Trans. Terahertz Sci. Technol.* **2015**, *5*, 645–648. [CrossRef]
18. Hou, L.; Tang, S.; Hou, B.; Marsh, J.H. Photonic integrated circuits for terahertz source generation. *IET Optoelectron.* **2020**, *14*, 136–142. [CrossRef]
19. Köhler, R.; Tredicucci, A.; Beltram, F.; Beere, H.E.; Linfield, E.H.; Davies, A.G.; Ritchie, D.A.; Iotti, R.C.; Rossi, F. Terahertz semiconductor-heterostructure laser. *Nature* **2002**, *417*, 156–159. [CrossRef] [PubMed]
20. Ishibashi, T.; Shimizu, N.; Kodama, S.; Ito, H.; Nagatsuma, T.; Furuta, T. Uni-Traveling-Carrier Photodiodes. In *Ultrafast Electronics and Optoelectronics*; Nuss, M., Bowers, J., Eds.; OSA Trends in Optics and Photonics Series; Optica Publishing Group: Incline Village, NV, USA, 1997; Volume 13, p. UC3.

21. Morales, A.; Nazarikov, G.I.; Rommel, S.; Okonkwo, C.; Monroy, I.T. All-Photonic Heterodyne sub-THz Wireless Transmission at 80 GHz, 120 GHz and 160 GHz Carrier Frequencies. In Proceedings of the 2020 45th International Conference on Infrared, Millimeter, and Terahertz Waves (IRMMW-THz), Buffalo, NY, USA, 8–13 November 2020; pp. 1–2.
22. García-Muñoz, E.; Abdalmalak, K.A.; Santamaría, G.; Rivera-Lavado, A.; Segovia-Vargas, D.; Castillo-Araníbar, P.; Van Dijk, F.; Nagatsuma, T.; Brown, E.R.; Guzman, R.C.; et al. Photonic-based integrated sources and antenna arrays for broadband wireless links in terahertz communications. *Semicond. Sci. Technol.* **2019**, *34*, 054001. [CrossRef]
23. Yang, H.; Zheng, S.; Zhang, H.; Li, N.; Shen, D.; He, T.; Yang, Z.; Lyu, Z.; Yu, X. A THz-OAM Wireless Communication System Based on Transmissive Metasurface. *IEEE Trans. Antennas Propag.* **2023**, *71*, 4194–4203. [CrossRef]
24. Carpenter, S.; Nopchinda, D.; Abbasi, M.; He, Z.S.; Bao, M.; Eriksson, T.; Zirath, H. A D-Band 48-Gbit/s 64-QAM/QPSK Direct-Conversion I/Q Transceiver Chipset. *IEEE Trans. Microw. Theory Tech.* **2016**, *64*, 1285–1296. [CrossRef]
25. Sawaby, M.; Dolatsha, N.; Grave, B.; Chen, C.; Arbabian, A. A fully packaged 130-GHz QPSK transmitter with an integrated PRBS generator. *IEEE Solid-State Circuits Lett.* **2018**, *1*, 166–169. [CrossRef]
26. Kim, Y.; Hu, B.; Huang, R.; Tang, A.; Joye, C.; Itoh, T.; Chang, M.C.F. 150-GHz CMOS TX/RX with Digitally Predistorted PAM-4 Modulation for Terahertz Contactless/Plastic Waveguide Communications. *IEEE Trans. Terahertz Sci. Technol.* **2020**, *10*, 370–382. [CrossRef]
27. Chen, L.; Taba, M.; Cathelin, A.; Afshari, E. A Low-Power 20Gb/s 196GHz BPSK Wireless Transmitter with Energy Efficiency FoM of 0.15pJ/bit/cm. In Proceedings of the Custom Integrated Circuits Conference (CICC), San Antonio, TX, USA, 23–26 April 2023; pp. 1–2.
28. Hagiwara, T.; Yamaki, N.; Sekine, K.; Sakai, H.; Sahara, K.; Takano, K.; Hara, S.; Lee, S.; Dong, R.; Tanoi, S.; et al. A 258-GHz CMOS Transmitter with Phase-Shifting Architecture for Phased-Array Systems. In Proceedings of the IIEEE MTT-S International Microwave Symposium (IMS), Atlanta, GA, USA, 7–25 June 2021; pp. 705–708.
29. Takiguchi, K. PAM4 wireless communication in 300 GHz-band using integrated-optic PAM signal emulator. In Proceedings of the 2022 Conference on Lasers and Electro-Optics (CLEO), San Jose, CA, USA, 15–20 May 2022; pp. 1–2.
30. Abdo, I.; Hamada, H.; Nosaka, H.; Shirane, A.; Okada, K. 64QAM wireless link with 300 GHz InP-CMOS hybrid transceiver. *IEICE Electron. Express* **2021**, *18*, 20210314. [CrossRef]
31. Pirrone, D.; Ferraro, A.; Zografopoulos, D.C.; Fuscaldo, W.; Szriftgiser, P.; Ducournau, G.; Beccherelli, R. Metasurface-Based Filters for High Data Rate THz Wireless Communication: Experimental Validation of a 14 Gbps OOK and 104 Gbps QAM-16 Wireless Link in the 300 GHz Band. *IEEE Trans. Wirel. Commun.* **2022**, *21*, 8688–8697. [CrossRef]
32. Nellen, S.; Lauck, S.; Peytavit, E.; Szriftgiser, P.; Schell, M.; Ducournau, G.; Globisch, B. Coherent Wireless Link at 300 GHz with 160 Gbit/s Enabled by a Photonic Transmitter. *J. Light. Technol.* **2022**, *40*, 4178–4185. [CrossRef]
33. Li, X.; Yu, J.; Wang, K.; Kong, M.; Zhou, W.; Zhu, Z.; Wang, C.; Zhao, M.; Chang, G.K. 120 Gb/s wireless terahertz-wave signal delivery by 375 GHz-500 GHz multi-carrier in a 2 × 2 MIMO system. *J. Light. Technol.* **2019**, *37*, 606–611. [CrossRef]
34. Shi, J.; Yu, J.; Zhang, J.; Zhu, M.; Zhang, L.; Liu, J.; Wang, K.; Zhou, W. 4096-QAM OFDM THz-over-fiber MIMO transmission using delta-sigma modulation. *IEEE Photonics Technol. Lett.* **2023**, *35*, 741–744. [CrossRef]
35. Rodriguez-Vazquez, P.; Grzyb, J.; Heinemann, B.; Pfeiffer, U.R. A QPSK 110-Gb/s Polarization-Diversity MIMO Wireless Link with a 220–255 GHz Tunable LO in a SiGe HBT Technology. *IEEE Trans. Microw. Theory Tech.* **2020**, *68*, 3834–3851. [CrossRef]
36. Liu, X.; Zhang, J.; Gao, S.; Tong, W.; Wang, Y.; Lei, M.; Hua, B.; Cai, Y.; Zou, Y.; Zhu, M. Demonstration of 144-Gbps Photonics-Assisted THz Wireless Transmission at 500 GHz Enabled by Joint DBN Equalizer. *Micromachines* **2022**, *13*, 1617. [CrossRef]
37. Yu, X.; Asif, R.; Piels, M.; Zibar, D.; Galili, M.; Morioka, T.; Jepsen, P.U.; Oxenløwe, L.K. 400-GHz Wireless Transmission of 60-Gb/s Nyquist-QPSK Signals Using UTC-PD and Heterodyne Mixer. *IEEE Trans. Terahertz Sci. Technol.* **2016**, *6*, 765–770. [CrossRef]
38. Nagatsuma, T.; Ducournau, G.; Renaud, C.C. Advances in terahertz communications accelerated by photonics. *Nat. Photonics* **2016**, *10*, 371–379. [CrossRef]
39. Yao, J.; Capmany, J. Microwave photonics. *Sci. China Inf. Sci.* **2022**, *65*, 314–335. [CrossRef]
40. Renaud, C.C.; Natrella, M.; Graham, C.; Seddon, J.; Van Dijk, F.; Seeds, A.J. Antenna integrated THz uni-traveling carrier photodiodes. *IEEE J. Sel. Top. Quantum Electron.* **2018**, *24*, 8500111. [CrossRef]
41. Shiramizu, T.; Seiki, N.; Matsumoto, R.; Masutomi, N.; Mikami, Y.; Ueda, Y.; Kato, K. Feasibility Demonstration of THz Wave Generation/Modulation Based on Photomixing Using a Single Wavelength-Tunable Laser. *Photonics* **2023**, *10*, 369. [CrossRef]
42. Tani, M.; Gu, P.; Hyodo, M.; Sakai, K.; Hidaka, T. Generation of coherent terahertz radiation by photomixing of dual-mode lasers. *Opt. Quantum Electron.* **2000**, *32*, 503–520. [CrossRef]
43. Kato, K. Photonics-Assisted Terahertz-Wave Beam Steering and Its Application in Secured Wireless Communication. *Photonics* **2022**, *9*, 9. [CrossRef]
44. Safian, R.; Ghazi, G.; Mohammadian, N. Review of photomixing continuous-wave terahertz systems and current application trends in terahertz domain. *Opt. Eng.* **2019**, *58*, 110901. [CrossRef]
45. Ishibashi, T.; Ito, H. Uni-traveling-carrier photodiodes. *J. Appl. Phys.* **2020**, *127*, 031101. [CrossRef]
46. Yoshimizu, Y.; Hisatake, S.; Kuwano, S.; Terada, J.; Yoshimoto, N.; Nagatsuma, T. Wireless transmission using coherent terahertz wave with phase stabilization. *IEICE Electron. Express* **2013**, *10*, 20130578. [CrossRef]
47. Gonzalez-Guerrero, L.; Carpintero, G. Coherent photonic Terahertz transmitters compatible with direct comb modulation. *Sci. Rep.* **2022**, *12*, 9526. [CrossRef] [PubMed]

48. Sakuma, K.; Takeuchi, S.; Fujimura, Y.; Haruki, J.; Kato, K.; Hisatake, S.; Nagatsuma, T. First demonstration of Mach-Zehnder-interferometric phase-stabilization at optoelectronic carrier generation for phase-shift keying signal. In Proceedings of the 2015 Opto-Electronics and Communications Conference (OECC), Shanghai, China, 28 June–2 July 2015; pp. 1–3.
49. Takeuchi, S.; Kato, K.; Yoshimizu, Y.; Yasuda, Y.; Hisatake, S.; Nagatsuma, T. Coherent sub-THz carrier frequency transmission with novel pseudo-Mach-Zehnder interferometric phase stabilization. In Proceedings of the Microwave Photonics (MWP) and the 2014 9th Asia-Pacific Microwave Photonics Conference (APMP) 2014 International Topical Meeting on, Hokkaido, Japan, 20–23 October 2014; pp. 208–210.
50. Takeuchi, S.; Sakuma, K.; Kato, K.; Yoshimizu, Y.; Yasuda, Y.; Hisatake, S.; Nagatsuma, T. Novel lightwave-interferometric phase detection for phase stabilization of two-tone coherent millimeter-wave/microwave carrier generation. *IEICE Trans. Electron.* **2016**, *E99C*, 1048–1055. [CrossRef]
51. Shiramizu, T.; Ibrahim, A.A.; Ye, S.; Mikami, Y.; Kato, K. Photonic Phase Stabilization Control System for Terahertz-Wave Phase Modulation. In Proceedings of the 2022 27th OptoElectronics and Communications Conference (OECC) and 2022 International Conference on Photonics in Switching and Computing (PSC), Toyama, Japan, 3–6 July 2022; pp. 1–4.